Materials Proceedings

MDPI

Proceeding Paper

Development of Polysilane-Inserted Perovskite Solar Cells †

Takeo Oku [1,*], Masaya Taguchi [1], Satsuki Kandori [1], Atsushi Suzuki [1], Masanobu Okita [2], Satoshi Minami [2], Sakiko Fukunishi [2] and Tomoharu Tachikawa [2]

[1] Department of Materials Science, The University of Shiga Prefecture, 2500 Hassaka, Hikone, Shiga 522-8533, Japan; of21mtaguchi@ec.usp.ac.jp (M.T.); os21skandori@ec.usp.ac.jp (S.K.); suzuki@mat.usp.ac.jp (A.S.)

[2] Osaka Gas Chemicals Co., Ltd., 5-11-61 Torishima, Konohana-ku, Osaka 554-0051, Japan; okita@ogc.co.jp (M.O.); s-minami@ogc.co.jp (S.M.); fukunishi@ogc.co.jp (S.F.); t-tachikawa@ogc.co.jp (T.T.)

* Correspondence: oku@mat.usp.ac.jp; Tel.: +81-749-28-8368

† Presented at the 2nd International Online-Conference on Nanomaterials, 15–30 November 2020; Available online: https://iocn2020.sciforum.net/.

Abstract: Perovskite solar cells, in which decaphenylcyclopentasilane (DPPS) layers were formed on the surface of a $CH_3NH_3PbI_3$-based perovskite layer, were developed. The photovoltaic properties were improved by controlling the annealing temperature of the perovskite layer. For perovskite layers annealed at high temperatures in the range of 180–220 °C, the perovskite crystals were densely formed and the surface coverage of the perovskite layer was improved. The DPPS-laminated devices suppressed the formation of PbI_2 crystals, and the stability was improved by the DPPS layer. Furthermore, the conversion efficiencies were improved over extended periods of time.

Keywords: polysilane; decaphenylcyclopentasilane; perovskite; photovoltaic device; solar cell; formamidinium; potassium

Citation: Oku, T.; Taguchi, M.; Kandori, S.; Suzuki, A.; Okita, M.; Minami, S.; Fukunishi, S.; Tachikawa, T. Development of Polysilane-Inserted Perovskite Solar Cells. *Mater. Proc.* **2021**, *4*, 51. https://doi.org/10.3390/IOCN2020-07834

Academic Editors: Ana María Díez-Pascual, Antonio Di Bartolomeo and Guanying Chen

Published: 11 November 2020

1. Introduction

The most commonly used solar cells are currently silicon-based solar cells. However, these silicon devices have a complicated fabrication process, and the silicon semiconductor has an indirect transition band structure. On the other hand, recently developed $CH_3NH_3PbI_3$ ($MAPbI_3$)-based perovskite compounds have demonstrated numerous advantages such as direct bandgaps, an easy fabrication process, and high conversion efficiencies [1,2]. Therefore, these compounds are considered to be major candidates for next-generation solar cell materials. However, these lead halide compounds are typically unstable in air, and the stability of the corresponding perovskite photovoltaic devices should be improved for inclusion in the actual cell module. The instability of perovskite photovoltaic devices results from the migration of CH_3NH_3 (MA) and iodine (I) and reactivity with H_2O [3,4].

To improve the stability of perovskite photovoltaic devices, polymeric materials have been investigated [5–7]. For instance, poly(methyl methacrylate) and poly(propylene carbonate) have been used to protect the perovskite layer from oxygen and moisture [8,9] and to enhance stability. Both polymeric materials formed cross-linked networks comprising perovskite grains, which suppressed defects. Furthermore, the stability was also influenced by hole transport layers (HTLs) [10]. In practice, 2,2′,7,7′-tetrakis(*N*,*N*-di-*p*-methoxyphenylamine)-9,9′-spirobifluorene (spiro-OMeTAD) is widely applied as a HTL for perovskite photovoltaic devices. However, this material is expensive, and the electronic properties degrade at elevated temperatures in air. Various alternative hole transport materials have been reported [11,12], and polysilane derivatives have also been investigated [13].

Polysilane derivatives exhibit two important advantages. The first relates to polysilanes being *p*-type semiconductors that facilitate hole transfer and rectification at the *pn* junction [13]. The second derives from polysilanes having high stabilities at elevated temperatures up to ~300 °C and are therefore expected to act as a protective layer across the perovskite surface. In addition, polysilanes have been applied to perovskite solar cells [14], and the photovoltaic properties were improved, especially by adding decaphenylcyclopentasilane (DPPS) [15,16]. The previously reported perovskite layers were a standard $MAPbI_3$ compound, so further studies focusing on doped $MAPbI_3$ compounds [17–19] are required to further elucidate the applicability of DPPS for perovskite solar cells.

Another method to improve the stability of perovskite solar cells is elemental or molecular doping of the perovskite crystals. The general formula of perovskite compounds is ABX_3, where A and B are cations and X is an anion. The perovskite crystal with a cubic system has the B cations in sixfold coordination, surrounded by an octahedron of X anions and the A cation in octahedral coordination. The perovskite crystal of $CH_3NH_3PbI_3$ is constructed with a Pb^{2+} cation at the B-site, I^- anion at the X-site, and $CH_3NH_3^+$ cation at the A-site. To estimate and predict the structural stabilities of the perovskite compounds, indicators called tolerance factors (*t*) have been calculated and used [19,20]. The tolerance factor is calculated as follows:

$$t = \frac{r_A + r_X}{\sqrt{2}(r_B + r_X)}, \quad (1)$$

where r_A, r_B, and r_X are the ionic radii of the A, B, and X ions. When *t* is close to 1, the perovskite structure is expected to be more structurally stable, although the ionic properties are not considered. The *t*-factor of $MAPbI_3$ is calculated to be 0.912 [19], and this indicates $MAPbI_3$ may be slightly unstable. To increase the *t*-factor and reduce the migration of MA, formamidinium (FA: $CH_3(NH_2)_2$) with a larger ionic radius (2.53 Å) than MA (2.17 Å) was doped at the MA site, and the stabilities of the perovskite solar cells were improved by FA addition [21,22]. Studies on devices with ethylammonium (EA: $CH_3CH_2NH_3$) [23,24] or guanidinium (GA: $C(NH_2)_3$) [25,26] additions to perovskites have also been reported. EA and GA have larger ionic radii (2.74 and 2.78 Å) than MA, and the addition of EA or GA can be expected to improve the structural stability from the viewpoint of the tolerance factors [19] and structural calculations [27,28]. It was reported that the crystallinity and stabilities of the perovskite crystals with EA were higher than those of ordinary $MAPbI_3$ [29]. Next, EA or GA addition to the perovskite compounds provided surface coatings with fewer defects, highly (100)-oriented crystals, and improved stability of the devices [24,26]. However, it should be noted that excessive addition of EA leads to phase separation, a decrease in crystallinity, and precipitation of PbI_2 as an impurity [30].

Since the above MA, FA, EA, and GA are molecules, they may affect the instabilities of the perovskite crystals. Therefore, substitution of alkali metal elements such as cesium (Cs), rubidium (Rb), potassium (K), and sodium (Na) might be effective for avoiding the migration and desorption of A-site elements in the perovskite crystals. It is also expected that the semiconductor characteristics of the perovskite crystals can be controlled by alkali element doping. Effects of Na and K doping to $MAPbI_3$ crystals on the electronic structures were investigated by first-principles calculation [31]. Partial substitution of MA with Na or K generated electronic orbitals of Na or K above the conduction band, which facilitated charge transfer from the alkali metals to the conduction band. This may then have accelerated carrier diffusion related to photovoltaic performances. Conversion efficiencies and stabilities were reported to be improved by adding Cs^+ and Rb^+ to perovskite precursor solutions, which increased grain sizes and reduced defect densities [32,33]. Conversion efficiencies were also improved by using K, which offered a lower cost than Rb and Cs. A calculated *t*-factor of K doping alone to $MAPbI_3$ indicated that the structural stability of perovskite compounds was reduced [19], and other cations with larger cationic radii, such as FA and EA, may have been necessary to form more stable perovskite structures.

The purpose of the present work is to investigate the photovoltaic properties and stabilities of DPPS-inserted $MAPbI_3$ perovskite solar cells doped with potassium (K) and formamidinium (FA), which are denoted as MA(FA,K)PbI_3. Previously, co-addition of K and FA was reported to be effective for enhancing photovoltaic properties [34–37]. In the present work, the $MAPbI_3$ and MA(FA,K)PbI_3 perovskite compounds, prepared at temperatures in the range of 180–220 °C in ambient air, were evaluated in terms of their photovoltaic properties and stability [38,39]. The effects of annealing temperatures and polysilane addition on the microstructures and photovoltaic properties of the MA(FA,K)PbI_3 perovskite solar cells were investigated using current density voltage (*J-V*) characteristics and X-ray diffraction (XRD).

2. Materials and Methods

A fabrication process of the present solar cell devices is schematically illustrated in Figure 1. The fabrication conditions were ~27 °C temperature and ~40% humidity in ambient air [40,41]. F-doped tin oxide (FTO, Nippon Sheet Glass Company, Tokyo, Japan, ~10 Ω/□) substrates were cleaned with methanol and acetone in an ultrasonic bath and an ultraviolet ozone cleaner (Asumi Giken, Tokyo, Japan, ASM401N) [18,42]. Next, 0.15 and 0.30 M precursor solutions of TiO_2 compact layers were prepared from 1-butanol (Wako Pure Chemical Industries, Osaka, Japan) and titanium diisopropoxide bis(acetylacetonate) (Sigma Aldrich, Tokyo, Japan). These precursor solutions of compact TiO_2 were spin-coated on the FTO substrate at 3000 rpm for 30 s, and the substrates were annealed at 125 °C for 5 min. To form a uniform, compact TiO_2 layer, the 0.30 M precursor solution was spin-coated twice. Next, the FTO substrate was annealed at 550 °C for 30 min to form the compact TiO_2 layer. After that, a TiO_2 paste (precursor solution for mesoporous TiO_2) was spin-coated on the compact TiO_2 layer at 5000 rpm for 30 s. This TiO_2 paste was prepared by mixing distilled water (0.5 mL), poly(ethylene glycol) PEG-20000 (Nacalai Tesque, Kyoto, Japan, PEG #20000, 20 mg), and TiO_2 powder (Aerosil, Tokyo, Japan, P-25, 200 mg). This solution was further mixed with the surfactant Triton X-100 (Sigma Aldrich, 10 μL) and acetylacetone (Wako Pure Chemical Industries, 20 μL) for 30 min, and it was left untouched for 24 h to remove bubbles in the solution [41]. To form the mesoporous TiO_2 layer, the TiO_2-coated substrates were annealed at 550 °C for 30 min.

The perovskite compounds were prepared by mixing *N*,*N*-dimethylformamide (DMF; Sigma Aldrich) solutions of KI (Wako Pure Chemical Industries), $HC(NH_2)_2I$ (Tokyo Chemical Industry, Tokyo, Japan), CH_3NH_3I (Tokyo Chemical Industry), and $PbCl_2$ (Sigma Aldrich) at 60 °C for 1 day. The basic precursor of $MAPbI_3$ was prepared with molar concentrations of $PbCl_2$ and MAI of 0.8 and 2.4 M, respectively [41,43], and $MA_{0.64}FA_{0.31}K_{0.05}PbI_3$ and $MA_{0.48}FA_{0.47}K_{0.05}PbI_3$ precursors were prepared by adding FAI and KI to control the desired molar ratio [38]. As the FA composition increased, the tolerance factor (*t*-factor) increased toward 1 [19], which indicated the crystal distortion in the perovskite structure could be reduced by FA addition. Perovskite precursor solutions were spin-coated on the mesoporous TiO_2 layer three times. For the first spin-coating, the perovskite solutions were spin-coated at 2000 rpm for 60 s. During the second and third spin-coatings, a hot air-blowing method was applied [19]. Temperatures of the cells during the air-blowing were set at 90 °C. A polysilane solution was prepared by mixing chlorobenzene (Fujifilm Wako Pure Chemical Corporation, 0.5 mL) with DPPS (Osaka Gas Chemicals, Osaka, Japan, OGSOL SI-30-10, 10 mg). During the last 15 s of the third spin-coating of the perovskite precursor solutions, the DPPS polysilane solution was also spin-coated on the perovskite layer [24]. The prepared cells were then annealed at 180 and 200 °C for 10 min and at 220 °C for 5 min in ambient air.

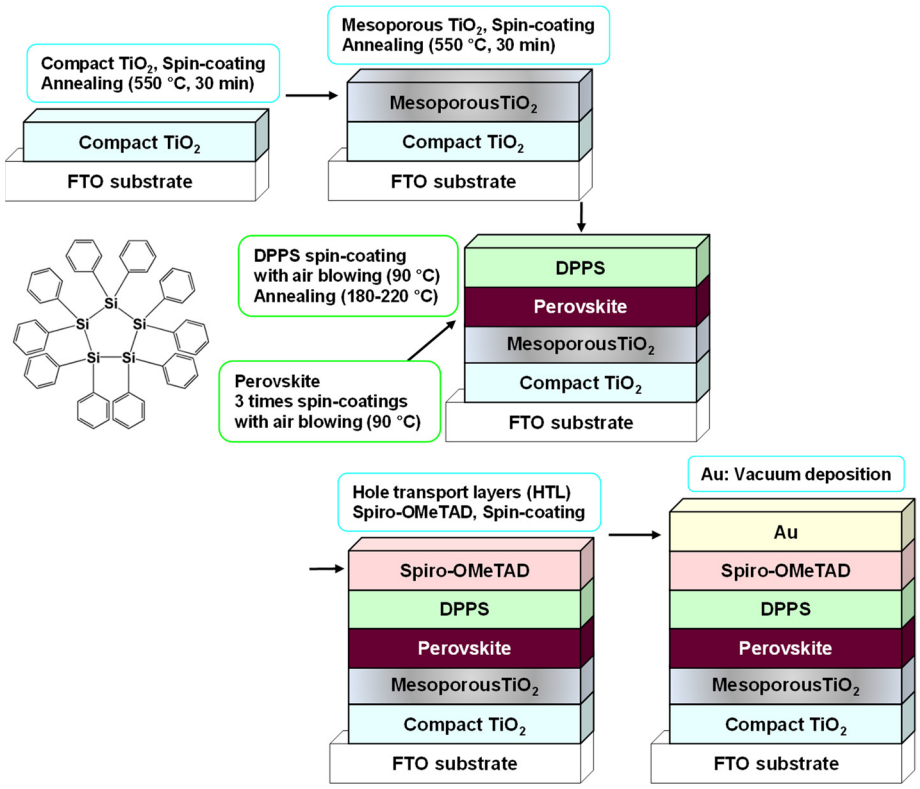

Figure 1. Schematic illustration detailing the processes adopted to fabricate the perovskite photovoltaic devices.

Hole transporting layers were spin-coated at 4000 rpm for 30 s. A precursor solution of the hole transporting layer was prepared by mixing chlorobenzene (0.5 mL; Wako Pure Chemical Industries, Osaka, Japan) and spiro-OMeTAD (Sigma Aldrich, St. Louis, MO, USA, 36.1 mg) for 24 h. An acetonitrile (Nacalai Tesque, Kyoto, Japan, 0.5 mL) solution of lithium bis(trifluoromethylsulfonyl)imide (Tokyo Chemical Industry, 260 mg) was similarly prepared by 24 h stirring. This lithium bis(trifluoromethylsulfonyl)imide solution (8.8 μL) was added to the spiro-OMeTAD solution mixed with 4-*tert*-butylpyridine (Sigma Aldrich, 14.4 μL) and stirred at 70 °C for 30 min. Lastly, top-electrodes of gold (Au) were formed by a vacuum evaporating system (Sanyu Electron, Tokyo, Japan, SVC-700TMSG). All the fabricated devices were stored at 22 °C and ~30% humidity in ambient air.

The current density voltage characteristics (Keysight, Santa Rosa, CA, USA, B2901A) of the fabricated devices were measured under a solar-simulating light source (San-ei Electric, Osaka, Japan, XES-301S) operated at 100 mW cm^{-2} (air mass 1.5). The exposed area of the photovoltaic devices was 0.080 cm^2. An X-ray diffractometer (Bruker, Billerica, MA, USA, D2 PHASER) was used for microstructural analysis of the perovskite crystals.

3. Results and Discussion

Figure 2 shows conversion efficiency changes of the $MA_{0.64}FA_{0.31}K_{0.05}PbI_3$ devices prepared at 180–220 °C. For the as-prepared devices, those annealed at 200 °C showed the highest conversion efficiency of ~11% and were almost identical to the conversion efficiency after 163 days. For the device annealed at 220 °C, the conversion efficiencies decreased after 50 days. For the device prepared at 180 °C, the conversion efficiency was observed at 1.67%. After 42 days, the open-circuit voltage and short-circuit current density were improved. Furthermore, the fill factor also improved after 131 days. After 163 days, the photovoltaic properties of the $MA_{0.64}FA_{0.31}K_{0.05}PbI_3$ device were further enhanced [38], and the highest conversion efficiency of 13.82% was obtained, as shown in Figure 2.

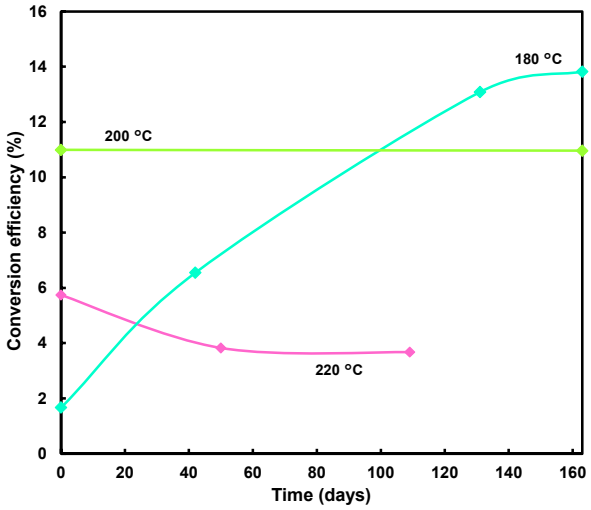

Figure 2. Changes of conversion efficiencies of $MA_{0.64}FA_{0.31}K_{0.05}PbI_3$ photovoltaic devices prepared at 180, 200, and 220 °C.

XRD patterns of the perovskite solar cells showed highly (100)-oriented crystals of the perovskite compounds, which were formed by the hot air-blowing method [19]. All devices presented few peaks corresponding to PbI_2, which indicated the effectiveness of the DPPS layer against high-temperature annealing at ~200 °C. Almost no PbI_2 formation was observed for the $MA_{0.48}FA_{0.47}K_{0.05}PbI_3$ devices, even after annealing at 220 °C. The FA-rich composition contributed to the stability of the cubic perovskite and suppressed PbI_2 formation.

A schematic model showing the microstructures, carrier dynamics, and stability of the proposed devices is shown in Figure 3a. As there was no DPPS layer for the standard device, the perovskite compound decomposed to PbI_2 after several months through the desorption of CH_3NH_3 and influences of oxygen and H_2O in the air. The number of holes and electrons generated in the perovskite layer was therefore reduced, and the photovoltaic properties were degraded. However, the stability of the $MAPbI_3$/(DPPS) devices improved because DPPS functioned as a protective layer and suppressed decomposition of the perovskite compound. From the XRD results, the peak intensity of 100 perovskite increased after several months. The number of electrons and holes generated in the perovskite layer therefore increased, and the photovoltaic properties were slightly improved after several months.

In the present work, chlorobenzene was used as the solvent for the DPPS solution. Chlorobenzene dripping is often used to improve not only crystallinity of perovskite films but also photovoltaic performance of perovskite solar cells [44,45]. Although the annealing temperature of 100 °C is enough for the chlorobenzene-dripped devices, the higher annealing temperature of ~200 °C is necessary for the present DPPS-dripped device. This indicates that the improvement mechanism of the photovoltaic properties would be different from that of the chlorobenzene dripping. The DPPS layer could work as the effective protective layer, improving the stability. In addition, the DPPS with the hole transport property would suppress the charge recombination and improve the photovoltaic properties. To explain the charge transport, an energy-level diagram of the FTO/TiO_2/Perovskite/(DPPS)/Spiro-OMeTAD/Au photovoltaic devices is shown in Figure 3b. Previously reported values are used as the energy levels [46,47]. By irradiating light from the FTO substrate side, electrons and holes were generated in the perovskite layer. Electrons generated in the photoactive layer were transported through TiO_2 to the FTO, and holes were transported through DPPS and spiro-OMeTAD to the Au. By incorporating DPPS between the perovskite and HTL, effective hole transport from the valence band of the perovskite to the Au electrode was induced. This smooth transport was also due to the molecular structure of DPPS [13,16,38].

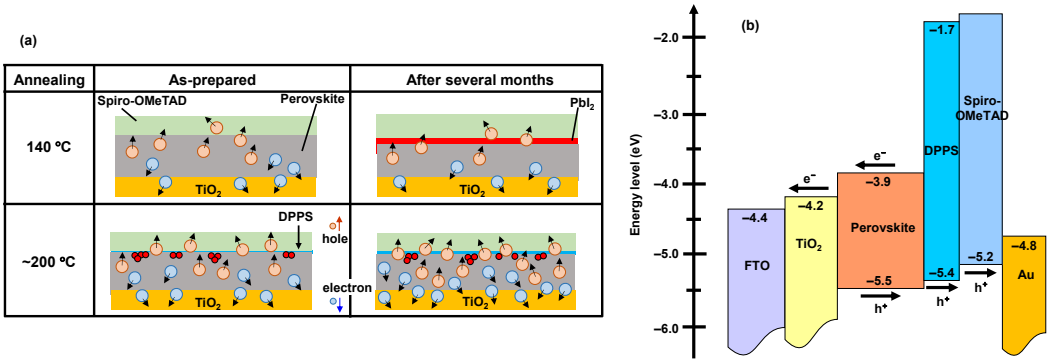

Figure 3. (**a**) Schematic illustration of microstructures, carrier dynamics, and stability for perovskite solar cells under different annealing temperatures. (**b**) Energy level diagram of the cell.

4. Conclusions

In summary, the effects on photovoltaic properties of inserting a DPPS layer between the perovskite layer and HTL were investigated. The *J-V* characteristics indicated improvements to the devices upon introducing a DPPS layer on the perovskite layer after annealing at high temperatures. The device annealed at 200–220 °C showed the highest conversion efficiencies among the as-prepared devices. On the other hand, the photovoltaic properties of the device annealed at 180 °C were improved after several months. Microstructures of the perovskite compounds were investigated by XRD, which indicated suppression of PbI_2 formation for the DPPS-added device formed at 180 °C, even after six months. Increased crystallite sizes of the perovskite promoted a decrease of the grain boundary area and point defects, which reduced the current leakage and improved the photovoltaic performance. The present results indicate that polysilane insertion and high-temperature annealing are effective for the improvement of the conversion efficiencies of perovskite photovoltaic devices.

Author Contributions: Conceptualization, T.O., M.T., and S.K.; Methodology, T.O., M.T., S.K., and A.S.; Formal Analysis, T.O., M.T., and S.K.; Investigation, S.K.; Resources, M.O., S.M., S.F., and T.T.; Data Curation, T.O., M.T., and S.K.; Writing—Original Draft Preparation, T.O.; Writing—Review & Editing, M.T., S.K., A.S., M.O., S.M., S.F., and T.T.; Project Administration, T.O.; Funding Acquisition, T.O. All authors have read and agreed to the published version of the manuscript.

Funding: A part of the present study was supported by the Japan Science and Technology Agency (JST).

Institutional Review Board Statement: Not applicable.

Informed Consent Statement: Not applicable.

Data Availability Statement: Data is contained within the article.

Conflicts of Interest: The authors declare no conflict of interest.

References

1. Miyasaka, T.; Kulkarni, A.; Kim, G.M.; Öz, S.; Jena, A.K. Perovskite solar cells: Can we go organic-free, lead-free, and dopant-free? *Adv. Energy Mater.* **2020**, *10*, 1902500, doi:10.1002/aenm.201902500.
2. Tong, J.; Song, Z.; Kim, D.M.; Chen, X.; Chen, C.; Palmstrom, A.F.; Ndione, P.F.; Reese, M.O.; Dunfield, S.P.; Reid, O.G.; et al. Carrier lifetimes of >1 μs in Sn-Pb perovskites enable efficient all-perovskite tandem solar cells. *Science* **2019**, *364*, 475–479, doi:10.1126/science.aav7911.
3. Dunfield, S.P.; Bliss, L.; Zhang, F.; Luther, J.M.; Zhu, K.; van Hest, M.F.A.M.; Reese, M.O.; Berry, J.J. From defects to degradation: A mechanistic understanding of degradation in perovskite solar cell devices and modules. *Adv. Energy Mater.* **2020**, *10*, 1904054, doi:10.1002/aenm.201904054.
4. Lee, J.W.; Kim, S.G.; Yang, J.M.; Yang, Y.; Park, N.G. Verification and mitigation of ion migration in perovskite solar cells. *APL Mater.* **2019**, *7*, 041111, doi:10.1063/1.5085643.
5. Bi, D.; Yi, C.; Luo, J.; Decoppet, J.D.; Zhang, F.; Zakeeruddin, S.M.; Li, X.; Hagfeldt, A.; Gratzel, M. Polymer-templated nucleation and crystal growth of perovskite films for solar cells with efficiency greater than 21%. *Nat. Energy* **2016**, *1*, 16142, doi:10.1038/nenergy.2016.142.

6. Zuo, L.; Guo, H.; deQuilettes, D.W.; Jariwala Marco, S.N.D.; Dong, S.; De Block, R.; Ginger, D.S.; Dunn, B.; Wang, M. Polymer-modified halide perovskite films for efficient and stable planar heterojunction solar cells. *Sci. Adv.* **2017**, 3, e1700106, doi:10.1126/sciadv.1700106.
7. Zhang, H.; Shi, J.; Zhu, L.; Luo, Y.; Li, D.; Wu, H.; Meng, Q. Polystyrene stabilized perovskite component, grain and microstructure for improved efficiency and stability of planar solar cells. *Nano Energy* **2018**, *43*, 383–392, doi:10.1016/j.nanoen.2017.11.024.
8. Wang, F.; Shimazaki, A.; Yang, F.; Kanahashi, K.; Matsuki, K.; Miyauchi, Y.; Takenobu, T.; Wakamiya, A.; Murata, Y.; Matsuda, K. Highly efficient and stable perovskite solar cells by interfacial engineering using solution-processed polymer layer. *J. Phys. Chem. C* **2017**, *121*, 1562−1568, doi:10.1021/acs.jpcc.6b12137.
9. Han, T.H.; Lee, J.W.; Choi, C.; Tan, S.; Lee, C.; Zhao, Y.; Dai, Z.; Marco, N.D.; Lee, S.J.; Bae, S.H.; et al. Perovskite-polymer composite cross-linker approach for highly-stable and efficient perovskite solar cells. *Nat. Commun.* **2019**, *10*, 520, doi:10.1038/s41467-019-08455-z.
10. Kim, G.W.; Choi, H.; Kim, M.; Lee, J.; Son, S.Y.; Park, T. Hole transport materials in conventional structural (*n–i–p*) perovskite solar cells: From past to the future. *Adv. Energy Mater.* **2020**, *10*, 1903403, doi:10.1002/aenm.201903403.
11. Tavakoli, M.M.; Tavakoli, R.; Prochowicz, D.; Yadav, P.; Saliba, M. Surface modification of a hole transporting layer for an efficient perovskite solar cell with an enhanced fill factor and stability. *Mol. Syst. Des. Eng.* **2018**, *3*, 717–722, doi:10.1039/C8ME00036K.
12. Mabrouk, S.; Zhang, M.; Wang, Z.; Liang, M.; Bahrami, B.; Wu, Y.; Wu, J.; Qiao, Q.; Yang, S. Dithieno[3,2-b:2′,3′-d]pyrrole-based hole transport materials for perovskite solar cells with efficiencies over 18%. *J. Mater. Chem. A* **2018**, *6*, 7950−7958, doi:10.1039/C8TA01773E.
13. Oku, T.; Nakagawa, J.; Iwase, M.; Kawashima, A.; Yoshida, K.; Suzuki, A.; Akiyama, T.; Tokumitsu, K.; Yamada, M.; Nakamura, M. Microstructures and photovoltaic properties of polysilane-based solar cells. *Jpn. J. Appl. Phys.* **2013**, *52*, 04CR07, doi:10.7567/JJAP.52.04CR07.
14. Shirahata, Y.; Yamamoto, Y.; Suzuki, A.; Oku, T.; Fukunishi, S.; Kohno, K. Effects of polysilane-doped spiro-OMeTAD hole transport layers on photovoltaic properties. *Phys. Status Solidi A* **2017**, *214*, 1600591, doi:10.1002/pssa.201600591.
15. Taguchi, M.; Suzuki, A.; Oku, T.; Fukunishi, S.; Minami, S.; Okita, M. Effects of decaphenylcyclopentasilane addition on photovoltaic properties of perovskite solar cells. *Coatings* **2018**, *8*, 461, doi:10.3390/coatings8120461.
16. Oku, T.; Nomura, J.; Suzuki, A.; Tanaka, H.; Fukunishi, S.; Minami, S.; Tsukada, S. Fabrication and characterization of $CH_3NH_3PbI_3$ perovskite solar cells added with polysilanes. *Int. J. Photoenergy* **2018**, *2018*, 8654963, doi:10.1155/2018/8654963.
17. Ueoka, N.; Oku, T.; Suzuki, A. Additive effects of alkali metals on Cu-modified $CH_3NH_3PbI_{3-\delta}Cl_\delta$ photovoltaic devices. *RSC Adv.* **2019**, *9*, 24231–24240, doi:10.1039/c9ra03068a.
18. Ueoka, N.; Oku, T. Effects of co-addition of sodium chloride and copper(II) bromide to mixed-cation mixed-halide perovskite photovoltaic devices. *ACS Appl. Energy Mater.* **2020**, *3*, 7272–7283, doi:10.1021/acsaem.0c00182.
19. Oku, T. Crystal structures of perovskite halide compounds used for solar cells. *Rev. Adv. Mater. Sci.* **2020**, *59*, 264–305, doi:10.1515/rams-2020-0015.
20. Tanaka, H.; Oku, T.; Ueoka, N. Structural stabilities of organic–inorganic perovskite crystals. *Jpn. J. Appl. Phys.* **2018**, *57*, 08RE12, doi:10.7567/JJAP.57.08RE12.
21. Zhou, Y.; Yang, M.; Pang, S.; Zhu, K.; Padture, N.P. Exceptional morphology-preserving evolution of formamidinium lead triiodide perovskite thin films via organic-cation displacement. *J. Am. Chem. Soc.* **2016**, *138*, 5535–5538, doi:10.1021/jacs.6b02787.
22. Suzuki, A.; Kato, M.; Ueoka, N.; Oku, T. Additive effect of formamidinium chloride in methylammonium lead halide compound-based perovskite solar cells. *J. Electron. Mater.* **2019**, *48*, 3900−3907, doi:10.1007/s11664-019-07153-2.
23. Wang, Y.; Zhang, T.; Li, G.; Xu, F.; Li, Y.; Yang, Y.; Zhao, Y. A mixed-cation lead iodide $MA_{1-x}EA_xPbI_3$ absorber for perovskite solar cells. *J. Energy Chem.* **2018**, *27*, 215–218, doi:10.1016/j.jechem.2017.09.027.
24. Nishi, K.; Oku, T.; Kishimoto, T.; Ueoka, N.; Suzuki, A. Photovoltaic characteristics of $CH_3NH_3PbI_3$ perovskite solar cells added with ethylammonium bromide and formamidinium iodide. *Coatings* **2020**, *10*, 410, doi:10.3390/coatings10040410.
25. Jodlowski, A.D.; Roldán-Carmona, C.; Grancini, G.; Salado, M.; Ralaiarisoa, M.; Ahmad, S.; Koch, N.; Camacho, L.; Miguel, G.; Nazeeruddin, M. Large guanidinium cation mixed with methylammonium in lead iodide perovskites for 19% efficient solar cells. *Nat. Energy* **2017**, *2*, 972–979, doi:10.1038/s41560-017-0054-3.
26. Kishimoto, T.; Suzuki, A.; Ueoka, N.; Oku, T. Effects of guanidinium addition to $CH_3NH_3PbI_{3-x}Cl_x$ perovskite photovoltaic devices. *J. Ceram. Soc. Jpn.* **2019**, *127*, 491−497, doi:10.2109/jcersj2.18214.
27. Liu, D.; Li, Q.; Wu, K. Ethylammonium as an alternative cation for efficient perovskite solar cells from first-principles calculations. *RSC Adv.* **2019**, *9*, 7356–7361, doi:10.1039/C9RA00853E.
28. Arkan, F.; Mohammad, I. Computational modeling of the photovoltaic activities in $EABX_3$ (EA = ethylammonium, B = Pb, Sn, Ge, X = Cl, Br, I) perovskite solar cells. *Comput. Mater. Sci.* **2018**, *152*, 324–330, doi:10.1016/j.commatsci.2018.06.006.
29. Zhang, F.; Cong, J.; Li, Y.; Bergstrand, J.; Liu, H.; Cai, B.; Hajian, A.; Yao, Z.; Wang, L.; Hao, Y.; et al. A facile route to grain morphology controllable perovskite thin films towards highly efficient perovskite solar cells. *Nano Energy* **2018**, *53*, 405–414, doi:10.1016/j.nanoen.2018.08.072.
30. Ueoka, N.; Oku, T.; Tanaka, H.; Suzuki, A.; Sakamoto, H.; Yamada, M.; Minami, S.; Miyauchi, S.; Tsukada, S. Effects of PbI_2 addition and TiO_2 electron transport layers for perovskite solar cells. *Jpn. J. Appl. Phys.* **2018**, *57*, 08RE05, doi:10.7567/JJAP.57.08RE05.

31. Suzuki, A.; Miyamoto, Y.; Oku, T. Electronic structures, spectroscopic properties, and thermodynamic characterization of sodium or potassium-incorporated $CH_3NH_3PbI_3$ by first principles calculation. *J. Mater. Sci.* **2020**, *55*, 9728–9738, doi:10.1007/s10853-020-04511-y.
32. Liu, C.; Kong, W.; Li, W.; Chen, H.; Li, D.; Wang, W.; Xu, B.; Cheng, C.; Jen, A.K.Y. Enhanced stability and photovoltage for inverted perovskite solar cells via precursor engineering. *J. Mater. Chem. A* **2019**, *7*, 15880–15886, doi:10.1039/c9ta03454d.
33. Zhang, M.; Yun, J.S.; Ma, Q.; Zheng, J.; Lau, C.F.J.; Deng, X.; Kim, J.; Kim, D.; Seidel, J.; Green, M.A.; et al. High-efficiency rubidium-incorporated perovskite solar cells by gas quenching. *ACS Energy Lett.* **2017**, *2*, 438–444, doi:10.1021/acsenergylett.6b00697.
34. Zheng, F.; Chen, W.; Bu, T.; Ghiggino, K.P.; Huang, F.; Cheng, Y.; Tapping, P.; Kee, T.W.; Jia, B.; Wen, X. Triggering the passivation effect of potassium doping in mixed-cation mixed-halide perovskite by light illumination. *Adv. Energy Mater.* **2019**, *9*, 1901016, doi:10.1002/aenm.201901016.
35. Jalebi, M.A.; Garmaroudi, Z.A.; Pearson, A.J.; Divitini, G.; Cacovich, S.; Philippe, B.; Rensmo, H.; Ducati, C.; Friend, R.H.; Stranks, S.D. Potassium- and rubidium-passivated alloyed perovskite films: Optoelectronic properties and moisture stability. *ACS Energy Lett.* **2018**, *3*, 2671–2678, doi:10.1021/acsenergylett.8b01504.
36. Machiba, H.; Oku, T.; Kishimoto, T.; Ueoka, N.; Suzuki, A. Fabrication and evaluation of K-doped $MA_{0.8}FA_{0.1}K_{0.1}PbI_3$(Cl) perovskite solar cells. *Chem. Phys. Lett.* **2019**, *730*, 117–123, doi:10.1016/j.cplett.2019.05.050.
37. Kandori, S.; Oku, T.; Nishi, K.; Kishimoto, T.; Ueoka, N.; Suzuki, A. Fabrication and characterization of potassium- and formamidinium-added perovskite solar cells. *J. Ceram. Soc. Jpn.* **2020**, *128*, 805–811, doi:10.2109/jcersj2.20090.
38. Oku, T.; Kandori, S.; Taguchi, M.; Suzuki, A.; Okita, M.; Minami, S.; Fukunishi, S.; Tachikawa, T. Polysilane-inserted methylammonium lead iodide perovskite solar cells doped with formamidinium and potassium. *Energies* **2020**, *13*, 4776, doi:10.3390/en13184776.
39. Taguchi, M.; Suzuki, A.; Oku, T.; Ueoka, N.; Minami, S.; Okita, M. Effects of annealing temperature on decaphenylcyclopentasilane-inserted $CH_3NH_3PbI_3$ perovskite solar cells. *Chem. Phys. Lett.* **2019**, *737*, 136822, doi:10.1016/j.cplett.2019.136822.
40. Oku, T.; Zushi, M.; Imanishi, Y.; Suzuki, A.; Suzuki, K. Microstructures and photovoltaic properties of perovskite-type $CH_3NH_3PbI_3$ compounds. *Appl. Phys. Express* **2014**, *7*, 121601, doi:10.7567/APEX.7.121601.
41. Oku, T.; Ohishi, Y.; Ueoka, N. Highly (100)-oriented $CH_3NH_3PbI_3$(Cl) perovskite solar cells prepared with NH_4Cl using an air blow method. *RSC Adv.* **2018**, *8*, 10389–10395, doi:10.1039/c7ra13582c.
42. Oku, T.; Ohishi, Y.; Suzuki, A.; Miyazawa, Y. Effects of NH_4Cl addition to perovskite $CH_3NH_3PbI_3$ photovoltaic devices. *J. Ceram. Soc. Jpn*. **2017**, *125*, 303–307, doi:10.2109/jcersj2.16279.
43. Oku, T.; Ohishi, Y. Effects of annealing on $CH_3NH_3PbI_3$(Cl) perovskite photovoltaic devices. *J. Ceram. Soc. Jpn.* **2018**, *126*, 56−60, doi:10.2109/jcersj2.17162.
44. Jeon, N.J.; Noh, J.H.; Kim, Y.C.; Yang, W.S.; Ryu, S.; Seok, S. Solvent engineering for high-performance inorganic–organic hybrid perovskite solar cells. *Nat. Mater.* **2014**, *13*, 897–903, doi:10.1038/NMAT4014.
45. Xiao, M.; Huang, F.; Huang, W.; Dkhissi, Y.; Zhu, Y.; Etheridge, J.; Weale, A.G.; Bach, U.; Cheng, Y.B.; Spiccia, L. A fast deposition-crystallization procedure for highly efficient lead iodide perovskite thin-film solar cells. *Angew. Chem. Int. Ed.* **2014**, *53*, 9898–9903, doi:10.1002/anie.201405334.
46. Noh, J.H.; Im, S.H.; Heo, J.H.; Mandal, T.N.; Seok, S.I. Chemical management for colorful, efficient, and stable inorganic–organic hybrid nanostructured solar cells. *Nano Lett.* **2013**, *13*, 1764–1769, doi:10.1021/nl400349b.
47. Haga, Y.; Harada, Y. Photovoltaic characteristics of phthalocyanine-polysilane composite films. *Jpn. J. Appl. Phys.* **2001**, *40*, 855–861, doi:10.1021/nl400349b.